# Control of Reactivity and Regioselectivity for On-Surface Dehydrogenative Aryl−Aryl Bond Formation

Nemanja Kocić,*,[†] Xunshan Liu,[‡] Songjie Chen,[‡] Silvio Decurtins,[‡] Ondřej Krejčí,[§,∥] Pavel Jelínek,[§] Jascha Repp,[†] and Shi-Xia Liu*,[‡]

[†]Institute of Experimental and Applied Physics, University of Regensburg, 93053 Regensburg, Germany

[‡]Department of Chemistry and Biochemistry, University of Bern, 3012 Bern, Switzerland

[§]Institute of Physics of Czech Academy of Sciences, 16200 Prague, Czech Republic

[∥]Charles University in Prague, Faculty of Mathematics and Physics, Department of Surface and Plasma Science, 18000 Prague, Czech Republic

**ABSTRACT:** Regioselectivity is of fundamental importance in chemical synthesis. Although many concepts for site-selective reactions are well established for solution chemistry, it is not *a priori* clear whether they can easily be transferred to reactions taking place on a metal surface. A metal will fix the chemical potential of the electrons and perturb the electronic states of the reactants because of hybridization. Additionally, techniques to characterize chemical reactions in solution are generally not applicable to on-surface reactions. Only recent developments in resolving chemical structures by atomic force microscopy (AFM) and scanning tunneling microscopy (STM) paved the way for identifying individual reaction products on surfaces. Here we exploit a combined STM/AFM technique to demonstrate the on-surface formation of complex molecular architectures built up from a heteroaromatic precursor, the tetracyclic pyrazino[2,3-*f*][4,7]phenanthroline (**pap**) molecule. Selective intermolecular aryl−aryl coupling via dehydrogenative C−H activation occurs on Au(111) upon thermal annealing under ultrahigh vacuum (UHV) conditions. A full atomistic description of the different reaction products based on an unambiguous discrimination between pyrazine and pyridine moieties is presented. Our work not only elucidates that *ortho*-hydrogen atoms of the pyrazine rings are preferentially activated over their pyridine equivalents, but also sheds new light onto the participation of substrate atoms in metal−organic coordination bonding during covalent C−C bond formation.
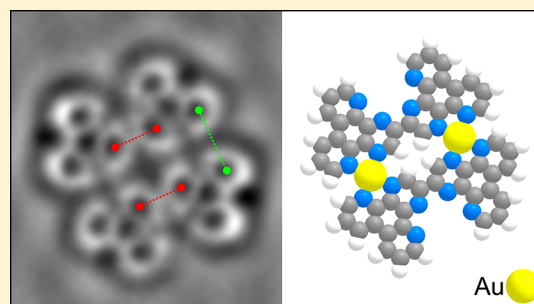
## INTRODUCTION

There are many synthetic protocols for the aryl−aryl bond formation, among which palladium-catalyzed cross-coupling chemistry is certainly most prominent in organic chemistry.[1] Nevertheless, the dehydrogenation, for instance between contiguous phenyls in phenylbenzenes, plays a similarly important role.[2] Notably the Scholl reaction,[3] the dehydrogenative coupling under the influence of a Lewis acid, has often been used for polyphenylene compounds, which are further converted to the corresponding polycyclic aromatic hydrocarbons (PAHs). These solution-based protocols paved the way for the preparation of a wide variety of π-extended PAHs by employing tailor-made oligophenylene precursors.[4] In a similar vein, noteworthy studies assessed whether the corresponding reaction mechanisms are based on the generation of a radical cation or an arenium cation. For example, Butenschön et al. initiated a discussion on the comparison of oxidative aromatic coupling and the Scholl reaction aiming to encourage further mechanistic studies.[5] Much less is known about a systematic examination on heterocyclic systems. Representative examples were exemplified by preparation of on N-doped nanographenes

and graphene nanoribbons via cyclodehydrogenation of a dipyrimidyl-substituted precursors.[6]

In contrast to the solution-based method, a complementary on-surface synthesis under UHV conditions enables the realization of unprecedented structures of PAHs that are otherwise unattainable.[7] A specific underlying growth mechanism has been described by Cai et al.[8] It demonstrates the occurrence of an Au(111) surface-assisted dehalogenation reaction of dibromo-bianthryl (C−C bond formation by Ullmann coupling) leading to linear polyphenylene chains at 200 °C which undergo a cyclodehydrogenation process upon annealing to 400 °C, yielding structurally perfect and fully π-conjugated carbon nanoribbons. Depending on the precursor molecules, on-surface preparation of this type provides access to graphene nanoribbons with different widths and edge structures,[9] including heteroatom-doped ones.[10] An intriguing question is, however, how a specific atomic configuration between reactant and metal catalyst controls the reaction process. In response, a recent study focused on the

dehalogenation and C−C coupling mechanisms of a polycyclic hydrocarbon compound on a metal substrate covered with a monolayer of hexagonal boron-nitride.[11] To summarize, a key insight from on-surface reactions is, that there are no inherent limitations for this strategy to be extended to more complex systems, as far as the necessary precursor monomers can be synthesized. In practical terms, however, finding new routes to fabricate complex heterostructures with for instance atomically precise N/C locations, still remains a challenge.[12]

A further important point is that the work, hitherto reported, does not yet adequately account for the possibility to steer catalytic regioselectivity,[13] means to favor bond formation at a particular atom over other possible atoms, into the class of surface-assisted reactions. The on-surface C−H bond scission is generally not regiospecific when the molecules contain several C−H bonds.[14] Very recently, one approach is given with an experimental and theoretical study on cyclodehydrogenation reactions of tetraphenylporphyrin (2H-TPP) molecules on Ag(111). It has been found that the 2-fold symmetry of the 2H-TPP's core, which is defined by the position of the H atoms, determines the selective reaction outcome.[13a] An alternative path for the regioselective formation of sophisticated structures is to apply a step-by-step connection of molecules which allows to connect them in a hierarchical manner by a selective and sequential activation of different sites on their perimeter.[15] To achieve selectivity, these reactive sites must be incorporated in the initial molecular building block. In conjunction with the catalytic selectivity issue, the work of Hanke et al. draws our attention to cooperative effects. Cyclodehydrogenation corresponds to positive cooperativity; hence, the probability of any given coupling is drastically increased if a neighboring coupling already exists.[16]

An important consensus is that significant progress in the field of on-surface synthesis has mainly been facilitated by single-molecule characterization techniques such as atomic force microscopy (AFM) and scanning tunneling microscopy (STM). Recently, the chemical structures of individual molecules have been resolved by AFM which was enabled by the functionalization of the tip.[17] This method has paved the way of identifying individual molecules on surfaces in various contexts,[18] and was soon after applied to in situ characterize and visualize on-surface chemical reaction products.[19]

In continuation of our current research focus on fused heterocyclic compounds[20] such as tetraazaperylene,[21] we set out to probe an even smaller tetraazapolycyclic precursor molecule, pyrazino[2,3-*f*][4,7]phenanthroline (**pap**),[22] for selective on-surface dehydrogenation and subsequent intermolecular C−C bond formation. This planar bis-N^N chelating molecule (Scheme 1) has so far exclusively been studied in the field of coordination chemistry acting as a bridging ligand to transition metal ions.[23] However, this heterocyclic molecule did draw our attention, first because its eight C−H bonds could be potentially differentiated in the dehydrogenative reaction pathways. Since two hydrogen atoms on the pyrazine ring may preferentially be activated over their pyridine equivalents, selective reaction sites are inherently incorporated. Second, subsequent intermolecular C−C bond formation can lead to larger heterocyclic compounds revealing atomically precise N/C locations. Here we present a combined STM/AFM investigation of an on-surface chemical reaction of the **pap** molecule under UHV conditions. This work demonstrates a clear discrimination between pyrazine and pyridine rings of the reaction products, thus giving convincing support for pyrazines'

**Scheme 1. Molecular Structure of Pyrazino[2,3-*f*][4,7]phenanthroline (pap) with Atom Numbering**[a]
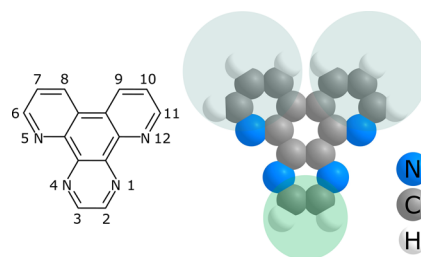


[a]Highlighting examples of potential sites for selective intermolecular C−C couplings via on-surface dehydrogenation.

inherent reactivity playing a key role in the regioselective aryl−aryl dehydrogenative coupling.

## ■ MATERIALS AND METHODS

**Chemicals.** Pyrazino[2,3-*f*][4,7]phenanthroline (**pap**) was synthesized as described previously.[22] The high yield is in the range of 80−90%.

**STM/AFM Measurements.** The experiments were carried out with a home-built combined STM/AFM operated in ultrahigh vacuum at a sample temperature of 6 K. The AFM is based on a qPlus tuning fork design (resonance frequency $f_0$ = 28.67 kHz, spring constant $k_0 \approx$ 1.8 × 10$^3$ N/m, quality-factor $Q \approx 10^4$, oscillation amplitude $A_{osc}$ = 50 pm,[24] and was operated in frequency-modulation mode. For FM-AFM measurements, the apex of the tip was functionalized with a CO molecule and the images were recorded at sample bias $V$ = 0 V by measuring the frequency shift while scanning in constant-height mode. After preparing a clean Au(111) surface from cyclic sputtering and annealing to 550 °C, **pap** molecules were deposited at a sample temperature below 10 K.

**Simulations.** The calculations of the free-standing molecules have been performed within the density functional theory (DFT) as implemented in the SIESTA code.[25] The calculations are based on both the local-density approximation (LDA) and the generalized gradient approximation (GGA). Core electrons are replaced by nonlocal norm-conserving pseudopotentials and valence electrons are described by linear combinations of numerical pseudoatomic orbitals. An energy cutoff of 400 Ry is employed and a double-$\zeta$ plus polarization basis set is used for the basis orbitals.

In addition, we performed total-energy DFT calculations using the FHI-aims code[26] to determine the adsorption geometry of **pap** molecules on a Au(111) surface. We carried out slab calculations: for the **pap** dimers optimization we employed a 8 × 8 supercell made of four Au layers to describe the Au(111) surface. From these, the three lower-most Au layers were kept fixed. A relaxation procedure was performed until the remaining atomic forces and changes of the total-energy were below 10$^{-2}$ eV/Å and 10$^{-5}$ eV, respectively. Only the Gamma point was used for the integration in the Brillouin zone. All the calculations were carried out at the GGA-PBE level including the Tkatchenko−Scheffler[27] treatment of the Van-der-Waals interactions.

To simulate the high-resolution AFM images, we used a mechanical probe-particle AFM model[28] including the electrostatic interaction.[29] The frequency shift was computed from the simulated $F(z)$-curves using Giessibl's formula[30] using the experimental values of $A_{osc}$ = 50 pm, $k_0 \approx$ 1.8 × 10$^3$ N/m and a lateral stiffness of the CO molecule of 0.5 N/m with an effective charge on the probe particle of −0.05 elementary charges (which is in agreement with our previously published results).

## ■ RESULTS AND DISCUSSION

The **pap** molecule was structurally characterized by single crystal X-ray measurement from its hydrated solid.[23c] It is virtually planar; the maximum atomic deviation from the least-
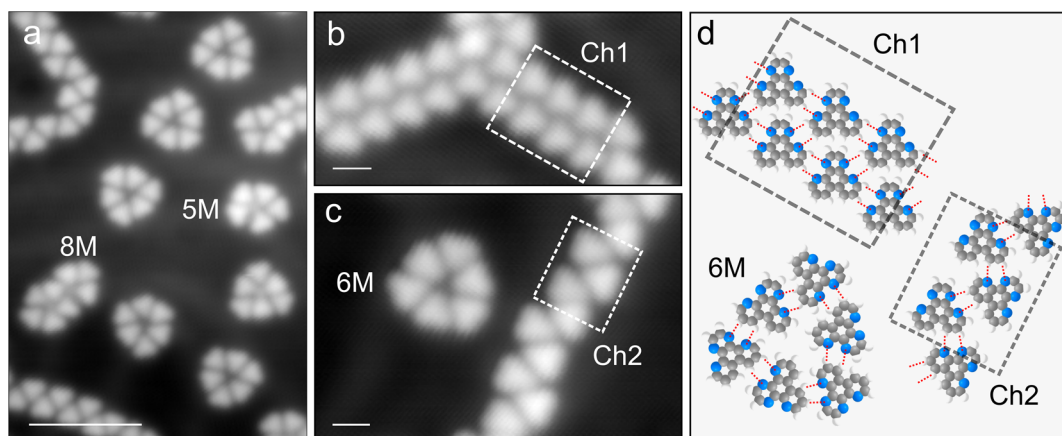
**Figure 1.** STM measurements of self-assembled hydrogen-bonded structures of pap molecules. (a–c) Typical self-assembled molecular clusters and (d) their proposed structure models with the same color code as in Scheme 1. Imaging parameters: $V = 0.3$ V, $I = 2$ pA. Scale bar: (a) 5 nm and (b,c) 1 nm.
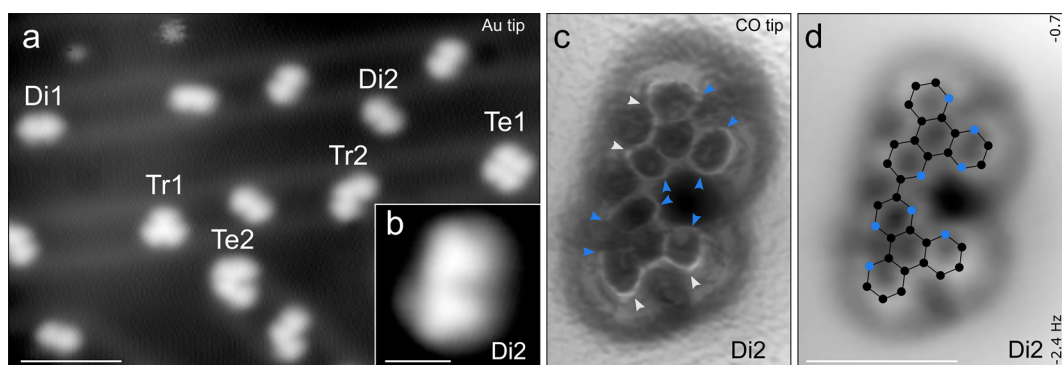


**Figure 2.** STM/AFM measurements of covalently bonded structures. (a) STM image showing several different dimer (Di1, Di2), trimer (Tr1, Tr2), and tetramer (Te1, Te2) structures. (b) STM image of one of a Di2-dimer structure. (c and d) AFM images of the same Di2-dimer as shown in (b). The same AFM-image is displayed twice with (c) and without (d) being high-pass filtered to highlight the molecular structure. The two **pap** molecules constituting the dimer can be readily identified. The distances between each two marked (arrow heads) atoms in every edge of the molecules appear quite differently in the images. From this, the carbon (long apparent distance, C8–C9, white) and nitrogen (short apparent distance, N4–N5 and N1–N12, blue) can be identified. On the basis of this identification the position of the edges including the nitrogen atoms can be identified from STM images as the ones exhibiting a smoother contrast transition. In (d) the resulting molecular structure is overlaid with black and blue circles as carbons and nitrogens, respectively. Imaging parameters: (a) $V = 0.3$ V, $I = 1$ pA. (b) $V = 0.05$ V, $I = 1$ pA. (c,d) $\Delta z = 1.33$ Å, $\Delta z$ corresponds to a distance decrease with respect to a STM set point of $I = 1$ pA, $V = 0.05$ V above the clean Au surface. Scale bar: (a) 5 nm and (b,d) 1 nm.

squares plane is 0.098 Å and the mean deviation is 0.05 Å. First, the self-assembly behavior of **pap** on the Au(111) surface was investigated. The molecules were deposited at a substrate temperature below 10 K and the sample surface was imaged after an annealing step to room temperature. As illustrated in Figure 1, STM images of the surface show an average coverage of approximately one molecule per 3 nm². As is immediately apparent, the molecules form different types of self-assembled structures, including small clusters but also longer chains of molecules. While the self-assembled structure formation is not the focus of this work, this observation proves that even at room-temperature the molecules have enough mobility to aggregate in self-assembled structures. All structures can be rationalized in terms of C–H···N hydrogen bonds formed between neighboring molecules.

To initiate the on-surface reaction, we annealed the sample to (410 ± 25) °C for 1 min. Figure 2a shows a typical STM image of the surface after the annealing. From this and many other STM images in total 166 clusters were observed. Six different types of clusters, namely dimers (Di1, Di2), trimers

(Tr1, Tr2), and tetramers (Te1, Te2) make up 94% of all structures, while no remaining monomers could be found on the surface. The limited size of clusters is in stark contrast to the self-assembled structures studied before the annealing step and a first hint toward the regioselectivity of the reaction. If all of the hydrogen sites would show the same reactivity, there would be no reason that no larger structures are formed as seen in the self-assembled structures. However, if one assumes that dehydrogenation mainly occurs at the pyrazine moiety of the molecule, clusters of limited size can be expected.

To gain information about the regioselectivity from AFM in real space, one has to be able to identify the different sites within the molecule; in the actual context a discrimination of pyridine from pyrazine is necessary. Whereas for phenazine adsorbed on a copper surface the nitrogen can readily be identified inside the molecule,[19a] this is not directly apparent in the present case. That the substrate may affect the appearance of atoms in adsorbed molecules in AFM images goes in line with simulations of the AFM-imaging process performed for graphene nanoribbons doped with boron atoms.[31] There it was
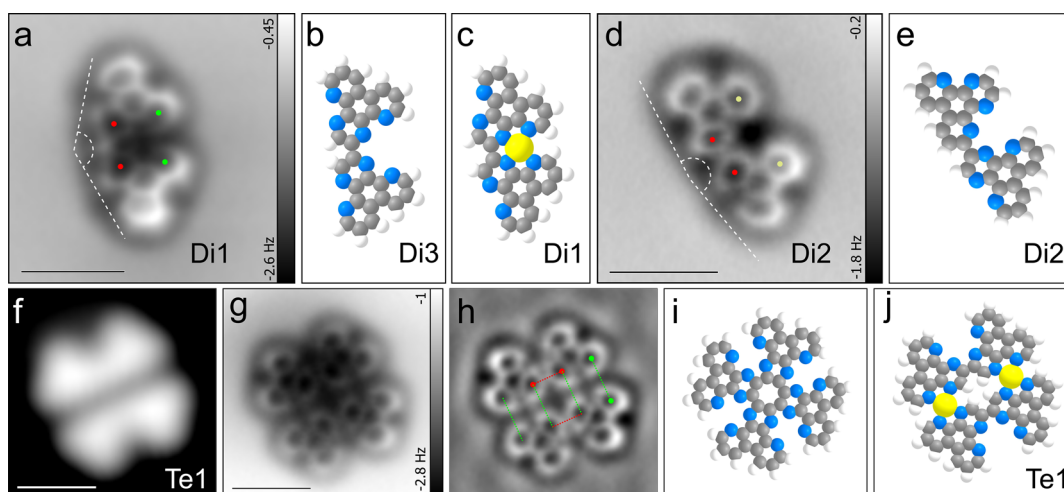
**Figure 3.** Detailed analysis of some of the observed molecular structures. (a and d) AFM images of a Di1- and a Di2-dimer, respectively. The distances between adjacent heterocycles (red and green dots) indicates that only one covalent bond was formed between each two **pap** constituents. The corresponding distance (red dots) of about 0.42 nm is in very good agreement to the distance expected for such a covalent bond. The main difference between the two dimer structures lies in the bond that has formed upon annealing (C2-to-C2 vs C2-to-C6). Another characteristic difference between the two dimer structures is the angle of alignment of the two **pap** constituents as indicated by the dashed lines in the images. Whereas the alignment in Di2 is consistent with just a covalent bond formation, the alignment observed in Di1 can only be rationalized if a stabilization of the dimer via metal coordination bonds is assumed, as shown in (c). Hence, the slightly shorter distance between adjacent heterocycles (green dots) of about 0.50 nm compared to the one of about 0.72 nm (yellow dots) we interpret as being indicative of a metal coordination bond being present. The appearance of the molecular structure allows one to identify the nitrogen atoms (see above) as shown in the corresponding models (b, c, and e). (f−j) STM (f), AFM (g), high-pass filtered AFM (h) image and structural models (i, j) of the Te1 tetramer. Based on the dimer analysis one readily observes distinctly different distances between adjacent heterocycles in Te1, indicating that Te1 consists of two dimer structures that are interconnected by metal coordination bonds to form the tetramer as illustrated in (j). Other possible structures as the one in (i) do not reproduce the distances and alignment angles of Te1. Imaging parameters: (a,d) $\Delta z = 1.33$ Å from $V = 0.05$ V, $I = 1$ pA. (g) $\Delta z = 1.9$ Å from $V = 0.2$ V, $I = 1$ pA. (f) STM image $V = 0.2$ V, $I = 1$ pA. Scale bars: 1 nm.

claimed that the difference in AFM contrast on boron atoms is only due to their different adsorption height as compared to carbon atoms. On the less reactive surface of Au(111) used here, it is therefore not surprising that no clear difference is observed. Nevertheless, the nitrogen sites can also be identified in the present case by two observations as follows.

Within the triphenylene backbone of the **pap** molecule at four of six distinct atomic positions the nitrogen atoms are incorporated. The C8−C9 distance is slightly larger than the N4−N5 and N1−N12. On top, image distortions in AFM imaging with CO functionalized tips may influence the apparent atomic distances.[32] Important in the current context is the prediction that electrostatic interactions contribute considerably to these distortions.[28] As the C−N bonds inside the molecule are expected to be slightly polar, AFM image distortions should slightly differ at the nitrogen and carbon positions in molecules. The distances between each two of these atomic positions in every edge of the molecules (see Figure 2c) appear quite differently in the images. The distance in one edge is particularly longer (3.5−4.0 Å) than those in the two other edges (2.3−2.9 Å). From this observation, the carbon (long apparent distance between C8−C9, white arrowheads) and nitrogen (short apparent distance between N4−N5 and N1−N12, blue arrowheads) can be identified. This assignment is supported by DFT calculations and AFM image simulations as will be discussed further below.

In STM images, each molecule appears as a triangular protrusion. When directly relating the STM and AFM images of the same individual structures, one realizes that the nitrogen-substituted edges - as determined from the AFM distortions - appear smoother than the ones without nitrogen. Whereas at one of its three edges the contrast falls off relatively abruptly, at the two other sides this transition is smoother. This correlation between STM contrast and AFM-image distortions further supports the assignment of nitrogen positions inside the molecules.

Being able to identify the positions of nitrogens as discussed above, we now turn to the discussion of bond formation in different structures. From atomically resolved AFM images we extracted structural information, namely, which intermolecular chemical bonds were formed. Figure 3a−e show the analysis of dimer structures. Irrespective of the AFM contrast indicating a covalent bond, the distances between adjacent heterocycles can be used as an indication of whether or not a bond is formed. The corresponding distance (red dots in Figure 3a,d) of (0.42 ± 0.03) nm is in excellent agreement to the distance expected for such a covalent bond. DFT calculations of the covalently bonded dimer structure without substrate yield the same distance of 0.42 nm. Both dimer structures indicate that only one covalent bond per dimer has been formed. In Di1 a bond has formed between two pyrazine moieties, namely a C2-to-C2-bond, according to the numbering introduced in Scheme 1. Di2, in contrast, involves a bond between a pyrazine and a pyridine moiety, a C2-to-C6-bond. We counted 101 dimers of type Di1 and 20 dimers of Di2 in our study, indicating the preference for pyrazine-bonded structures. Another characteristic difference between the two dimer structures is the alignment of the two **pap** constituents as indicated in Figure 3. Whereas the alignment in Di2 is consistent with just a covalent bond formation, the alignment observed in Di1 suggests that the different angle is due to a stabilization of the dimer via metal coordination bonding, as shown in Figure 3c. To corroborate this interpretation, we also performed DFT calculations of these structures, again excluding the substrate.
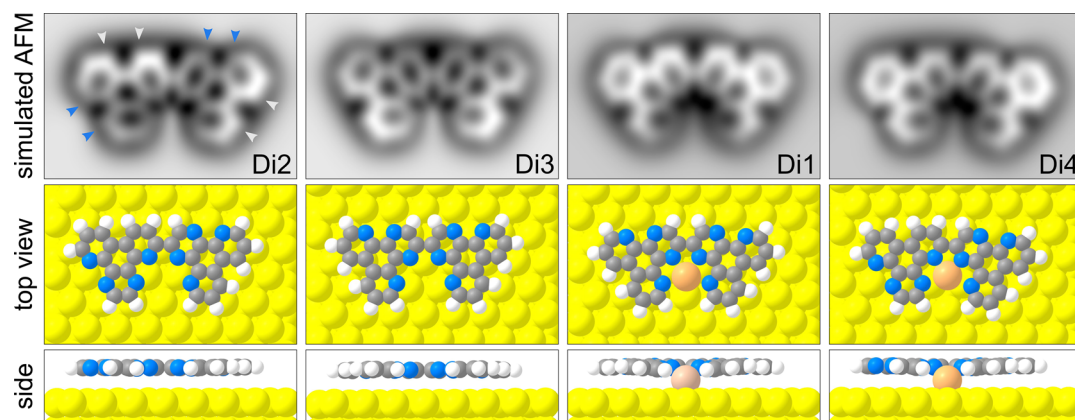
**Figure 4.** DFT-calculated structures and simulated AFM images. Pyrazine−pyrazine (C2-to-C2-bond, D1 and Di3) and pyrazine−pyridine (C2-to-C6-bond, Di2 and Di4) dimers, each with (Di1, Di4) and without (Di2, Di3) a gold adatom coordinated to nitrogens are shown in the calculated geometries. The corresponding simulated AFM images are shown above. The difference in the C8−C9 versus N4−N5 or N1−N12 distances (white and blue arrowheads, respectively) confirm the experimental assignment.

The DFT calculations reproduce the observed alignment angles (see Figure 3a,d) only if one includes or excludes a coordinating gold atom for Di1 and Di2, respectively. In particular, the slightly larger distance between the adjacent heterocycles that are not covalently bonded to each other (green dots in Di1) of (0.50 ± 0.03) nm is in qualitative agreement with the corresponding simulated structure (see Figure 3c). In contrast, if there is no metal coordination involved, the corresponding distance measures (0.72 ± 0.04) nm (yellow dots). We hence interpret this distance variation as being indicative of a metal coordination bond being present.[33] At first glance it is surprising that the gold atom is not directly visible in the AFM images—a circumstance that will be elucidated further below, after the analysis of tetramer Te1, shown in Figure 3f−j. On the surface it has $C_{2v}$ symmetry ($D_{2h}$ in the gas-phase) indicating that the bonds between the constituents are not all of the same nature. Following the reasoning from the dimer structure as outlined above, one immediately recognizes that Te1 consists of two dimers connected to each other via metal coordination bonds. This hypothesis is supported by DFT calculations carried out for the tetramer Te1 without substrate. Alternate models, e.g., assuming four covalent bonds, do not reproduce the experimentally observed structure.

We performed total-energy DFT calculations of four selected dimer structures including the substrate. Next we calculated AFM images of the corresponding optimized structures (see upper panel of Figure 4). Note that the image simulations take into account the bending of the CO molecule at the tip apex,[28,34] while the parameters required to simulate a CO tip were selected upon previous image simulations and their direct comparison to experimental data in other works.[35] To understand the possible participation of gold adatoms in metal−organic coordination bonding in our structures, we calculated not only Di1 and Di2, but two more dimers: The counterpart of Di1, but without a gold atom, henceforth labeled Di3, and the counterpart of Di2, but with an additional gold adatom, henceforth labeled Di4. Hence, these structures are pyrazine−pyrazine (C2-to-C2-bond, Di1 and Di3) and pyrazine−pyridine-bonded (C2-to-C6-bond, Di4 and Di2) dimers, each with and without a gold adatom coordinated to nitrogens. The relaxed geometries are shown in Figure 4, alongside with simulated AFM images. First we turn to the

discussion of C8−C9 versus N4−N5 and N1−N12 distances, relevant for the assignment of nitrogen positions in each molecule. The DFT calculation yields C8−C9-distances of 2.98−3.00 Å being distinctly larger than the N4−N5 and N1−N12 distances that measure only 2.69−2.78 Å. In the AFM imaging with a CO-terminated tip, this difference seems to be even exaggerated by distortions, such that in the simulated images it can be clearly discerned (see white and blue arrowheads) in agreement with the experiment. This puts the assignment of nitrogen positions inside the molecules from AFM images onto solid grounds.

The simulated images also confirm that it is possible to have a coordinating gold atom present in the structure without directly resolving it with the AFM as a repulsive feature. The reason for the absence of a repulsive feature from the gold adatom is related to (i) presence of charge transfer between the gold adatom and the molecule giving rise to an additional attractive interaction with CO-tip and to (ii) the vertical position of the gold adatom and the surrounding nitrogen atoms being considerably closer to the surface than the one of the organic framework, diminishing the onset of Pauli repulsion. Consequently, the gold atom leads to a dark circular halo of long-range attractive interaction. Indeed such a dark halo can also be seen in the experimental AFM image of Di1, for which we expect a gold adatom to be present, lending further support for the presence of a gold adatom.

What more, both dimer structures without gold adatom show a straight 180° alignment angle consistent with our interpretation of Di2. However, the angle of Di1 is about 170°, but not as small as the experimentally observed one. We also note that the experimental image of Di1 has a bright protrusion at the bond that formed upon annealing, which is not reproduced by the calculated AFM image, leaving some room for the interpretation of the atomistic details in Di1, in particular as it regards the exact position and bonding of an additional gold atom. We therefore conclude that the exact bonding geometry in Di1 is not fully captured by our DFT calculation. This can be ascribed to a deficiency in the description of metal−organic complexes by the DFT method.

In addition, we enforced alignment angles smaller than 180° for both, Di1 and Di3. We observed a considerable increase of the total-energy for both structures of few eV for angles smaller than 150°. We therefore exclude that the relatively weak
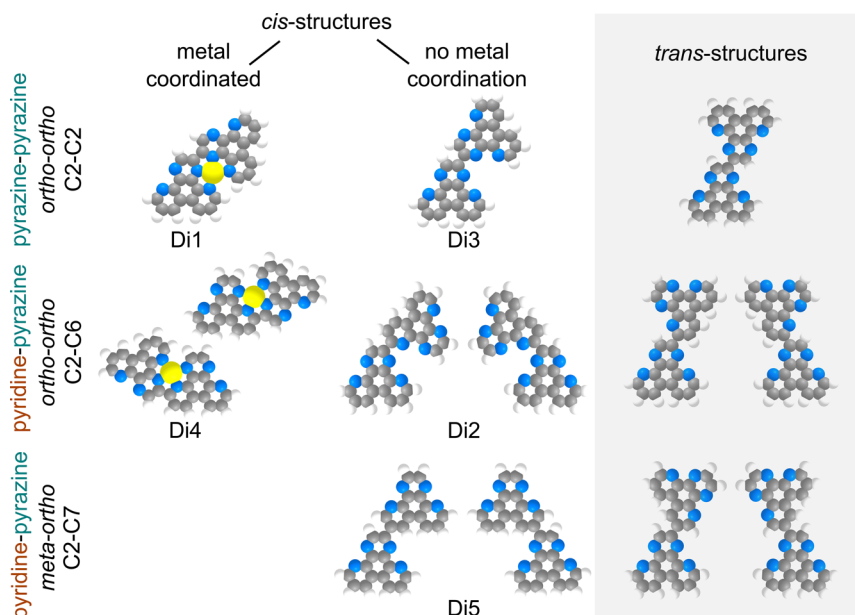
**Figure 5.** Possible structures of dimer formation. A covalent bond is formed either between *ortho*-carbon atoms of two pyrazine moieties (top row) or between a pyridine and a pyrazine moiety (center row) of the neighboring **pap** molecules. For the pyridine moiety also *meta*- and *para*-carbon atoms exist, which could react to form additional dimer structures exemplified for the *meta*-carbon (bottom row). For the pyridine-bonded structures, there are two enantiomers in each case. The bond configuration can be divided into *cis*-N^N and *trans*-N^N structures. Only the purely *ortho*-carbon bonded *cis*-N^N-structures facilitate metal coordination (Di1 and Di4).

interaction with a flat Au(111) surface without adatoms being present can enforce such a geometry. Our DFT calculations of molecules without a gold adatom revealed only weak, mostly van-der-Waals interaction with the Au(111) substrate underneath. Consequently, the molecules Di2 and Di3 adopt an almost planar configuration with the plane of the molecule located approximately 3.3 Å above the Au(111). The absence of a strong chemical bond between the molecule and the substrate exclude strong conformational changes of the molecules caused by the substrate.

Taking all the above observations into consideration, it is clear that the structural information from AFM images is decisive for the identification of all bonding configurations. However, after establishing the direct relationship between the geometric structure deduced from AFM and the appearances in STM images, one can identify the different type of structures also from the STM images alone. We note that this relationship between structure and appearance in STM images was established and confirmed on the basis of atomically resolved AFM images of in total 26 clusters. We therefore included also all highly resolved STM images in the statistical analysis discussed in the remainder of this work.

A covalent bond either between the two pyrazine moieties (Di1) or between a pyrazine and a pyridine moiety (Di2) of each two neighboring molecules was identified. Another difference between Di1 and Di2 lies in the metal coordination. However, irrespective of a possible metal coordination many more possibilities for a bond formation could be expected, even if regioselectivity is taking place. In this spirit, it is interesting to analyze, which dimer structures could possibly form and to compare that with the actual observations. Before doing so, we note that we never observed any structures involving covalent bonds between two pyridine moieties. We therefore largely exclude this possibility from the following discussion.

Figure 5 shows a set of dimer structures that could be envisioned. A covalent bond between pyridine and pyrazine

yields a dimer of lower symmetry than in the other case, which therefore may occur in two different enantiomers on the surface. Indeed we observe each two enantiomers in equal amounts within statistical significance. We disregard stereochemistry in the remainder of this work. Moreover, the covalent bond formation could result in either a *cis*-N^N or a *trans*-N^N configuration of the two **pap** constituents as exemplified in Figure 5. Considering the possible stabilization of the *trans*-configuration by intramolecular hydrogen bonds it is most surprising that we never observed any structures in *trans*-configuration of the molecules. This finding can be accounted for the fact that a *trans*-configuration could not be stabilized by a metal coordination bond. The same holds true for structures in which *meta*- and *para*-carbon atoms of a pyridine moiety are involved in the dimer formation: these would not facilitate metal coordination and we did not observe them. These two findings point toward an important role of metal coordination in the covalent bond formation. Figure 6 summarizes the possible dimer structures and their occurrences in the experiment. Although Di3 and Di4 were not observed at all as single entities in our study, reconsidering the tetramer Te1, one realizes that Te1 consists of two such Di3 dimers, which are linked via metal coordination bonds. Similarly, Di3 and Di4 dimers were observed as building blocks of larger clusters Tr2 and Te2, respectively (Figure 7). Interestingly, the highly symmetric Tr1 was formed based on a strict regioselectivity of the pyrazine groups of three neighboring **pap** molecules for dehydrogenation leading to the formation of a hexaazatriphenyl core. It constitutes due to its 3-fold symmetry and its N^N chelating property an established building block for a variety of applications.[20] Alternatively, Tr1 can be described as a three-star version of dipyrido[2,3-*a*:3′,2′-*c*]phenazine, a bridging ligand applied in coordination chemistry.[36]

Figure 7 shows an overview of the most probable structures that were observed and also are the basis for the statistical analysis for regioselectivity. In total we observed 203 bonds that
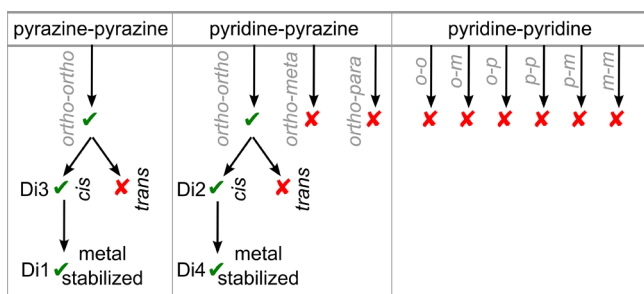
**Figure 6.** Hierarchy of dimer structures. Dimer structures can be classified according to the bonding moiety (top row), to their bonding positions (second row), relative orientation (third row), and additional metal coordination (bottom row). Structures observed in the experiments are checked, all others crossed, highlighting the strong selectivity of on-surface bond formation. The possibility of metal coordination seems to directly coincide with the respective structure being observed.

have been formed. Among them, 160 bonds occurred between two pyrazine moieties of each two neighboring molecules, 43 between a pyrazine and a pyridine group, and none between two pyridine groups,[37] demonstrating a very strong but not a extremely strict regioselectivity. Note that the latter statistics of the observation of different bond types is made irrespective of whether Au adatoms are involved or not. As each **pap** molecule consists of two pyridine but only one pyrazine moiety, in absence of any regioselectivity one would expect a ratio of occurrences of 1:4:4 of bond-types pyrazine−pyrazine:pyrazine−pyridine:pyridine−pyridine, which is quite opposite to what is observed. When being interpreted in terms of thermodynamic equilibrium at 200 °C and the Boltzmann statistics, the observed occurrences would yield an energy difference of $\Delta E \simeq 2.6$ kcal/mol of pyrazine−pyrazine versus pyrazine−pyridine bonding geometry.

We would like to mention, that some of the images show apparent bonds between neighboring nitrogen atoms. However, such features have been observed before and were identified as imaging artifacts.[34,38] In this context it is important to note that

the structural information deduced from the AFM images allows to unambiguously identify which moieties can be involved in the bonds from the molecules' orientations and the distances between heterocycles as presented above irrespective of where exactly real or apparent bonds are observed.

Although a thorough analysis of the mechanism behind our observations goes beyond the scope of this work, we now turn to a brief discussion of a *possible* mechanism behind one aspect of selective bond formation. As mentioned in the context of Figures 5 and 6, only *cis*-N^N-structures bonded in *ortho−ortho* geometry enable the incorporation of a gold atom, whereas *meta-ortho*-bonded *cis*-N^N-structures as well as all *trans*-N^N-structures do not. Hence, apparently exactly those structures are experimentally observed, which could potentially be stabilized by a coordinating gold atom. Such a gold atom may modify the reactivity of its direct neighborhood, facilitating dehydrogenation. More likely it appears to us, however, that it is rather the geometry that is important: a gold adatom between two monomers, will stabilize two hydrogens each belonging to a different monomer in close proximity, in which a concerted dehydrogenation and immediate bond formation may be facilitated. At the elevated temperature, the entire surface will be subject to constant change and rearrangement, but the presence of coordinating gold adatoms may favor certain geometries over others. When considering such a scenario, the importance of the molecular degrees of freedom being reduced to two dimensions in on-surface chemistry becomes apparent. Note that the regioselectivety concerning the preference for pyrazine-bonded structures observed for the ratio of occurences of different dimers cannot be accounted for by the above considerations alone. Hence, this is a separate aspect of our observations and must stem from a different reactivity of different sites. Thorough theoretical studies on the mechanism and the exact role of Au in these aryl−aryl couplings are ongoing in our laboratory.
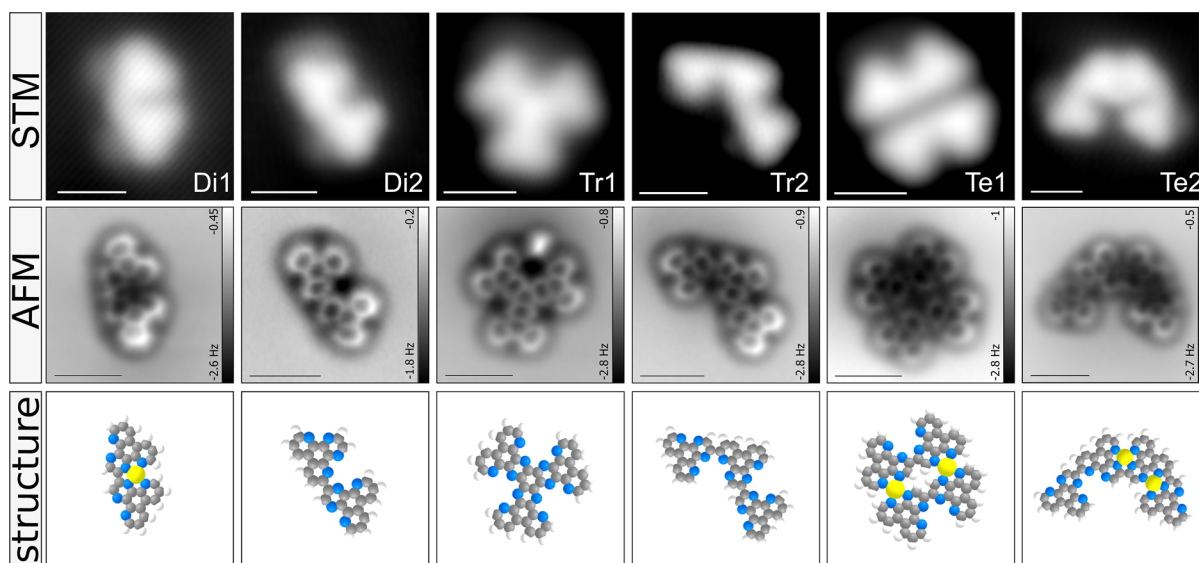


**Figure 7.** Analysis of main structures observed after covalent bond formation. STM images (top row), AFM images (middle row), and structures (bottom row) for products of dehydrogenation. The structural assignment follows the considerations discussed above.

## CONCLUSION

We have demonstrated that pyrazino[2,3-*f*][4,7]-phenanthroline (**pap**) can bond-selectively be transformed through aryl−aryl coupling on an Au(111) surface in UHV conditions into a variety of heterocyclic compounds. The observed regioselectivity of the reactions originates from the fact that *ortho*-hydrogen atoms of the pyrazine rings are preferentially activated for a dehydrogenative C−C bond formation over their pyridine equivalents. Most importantly, the combined STM/AFM study allows a full atomistic analysis of the different reaction products while unambiguously discriminating pyrazine from pyridine moieties. This synthetic strategy to utilize tailored polycyclic precursor molecules comprising pyrazine units will open an avenue for the construction of novel heterocyclic molecules. Depending on the number of pyrazine units incorporated into the starting molecule, the realization of more extended heteroaromatic structures with atomically precise nitrogen locations can be expected.

## AUTHOR INFORMATION

**Corresponding Authors**
*nemanja.kocic@ur.de
*liu@dcb.unibe.ch

**Notes**
The authors declare no competing financial interest.

## ACKNOWLEDGMENTS

## REFERENCES

(1) Bolm, C. *Org. Lett.* **2012**, *14*, 2925.

(2) Rempala, P.; Kroulík, J.; King, B. T. *J. Org. Chem.* **2006**, *71*, 5067.

(3) (a) Li, J. J. *Name Reactions: A Collection of Detailed Reaction Mechanism*, 2nd ed.; Springer-Verlag: New York, 2003. (b) Balaban, A. T.; Nenitzescu, C. D. *Dehydrogenating Condensations of Aromatics (Scholl and Related Reactions)*; Olah, G., Ed.; Wiley: New York, 1964; Vol. 2; pp 979−1047. (c) King, B. T.; Kroulík, J.; Robertson, C. R.; Rempala, P.; Hilton, C. L.; Korinek, J. D.; Gortari, L. M. *J. Org. Chem.* **2007**, *72*, 2279.

(4) (a) Simpson, C. D.; Brand, J. D.; Berresheim, A. J.; Przybilla, L.; Räder, H. J.; Müllen, K. *Chem. - Eur. J.* **2002**, *8*, 1424. (b) Simpson, C. D.; Mattersteig, G.; Martin, K.; Gherghel, L.; Bauer, R. E.; Räder, H. J.; Müllen, K. *J. Am. Chem. Soc.* **2004**, *126*, 3139. (c) Wu, J.; Pisula, W.; Müllen, K. *Chem. Rev.* **2007**, *107*, 718. (d) Narita, A.; Wang, X.-Y.; Feng, X.; Müllen, K. *Chem. Soc. Rev.* **2015**, *44*, 6616.

(5) Grzybowski, M.; Skonieczny, K.; Butenschön, H.; Gryko, D. T. *Angew. Chem., Int. Ed.* **2013**, *52*, 9900.

(6) (a) Gregg, D. J.; Bothe, E.; Höfer, P.; Passaniti, P.; Draper, S. M. *Inorg. Chem.* **2005**, *44*, 5654. (b) Wijesinghe, L. P.; Lankage, B. S.; Máille, G. M. Ó; Perera, S. D.; Nolan, D.; Wang, L.; Draper, S. M. *Chem. Commun.* **2014**, *50*, 10637. (c) Vo, T. H.; Shekhirev, M.; Kunkel, D. A.; Orange, F.; Guinel, M. J.-F.; Enders, A.; Sinitskii, A. *Chem. Commun.* **2014**, *50*, 4172.

(7) (a) Méndez, J.; López, M. F.; Martín-Gago, J. A. *Chem. Soc. Rev.* **2011**, *40*, 4578. (b) Franc, G.; Gourdon, A. *Phys. Chem. Chem. Phys.* **2011**, *13*, 14283. (c) El Garah, M.; MacLeod, J. M.; Rosei, F. *Surf. Sci.* **2013**, *613*, 6. (d) Wiengarten, A.; Seufert, K.; Auwärter, W.; Écija, D.; Diller, K.; Allegretti, F.; Bischoff, F.; Fischer, S.; Duncan, D. A.; Papageorgiou, A. C.; Klappenberger, F.; Acres, R. G.; Ngo, T. H.; Barth, J. V. *J. Am. Chem. Soc.* **2014**, *136*, 9346. (e) Sun, Q.; Zhang, C.; Cai, L.; Xie, L.; Tan, Q.; Xu, W. *Chem. Commun.* **2015**, *51*, 2836. (f) Dong, L.; Liu, P. N.; Lin, N. *Acc. Chem. Res.* **2015**, *48*, 2765. (g) Fan, Q.; Gottfried, J. M.; Zhu, J. *Acc. Chem. Res.* **2015**, *48*, 2484.

(8) Cai, J.; Ruffieux, P.; Jaafar, R.; Bieri, M.; Braun, T.; Blankenburg, S.; Muoth, M.; Seitsonen, A. P.; Saleh, M.; Feng, X.; Müllen, K.; Fasel, R. *Nature* **2010**, *466*, 470.

(9) (a) Blankenburg, S.; Cai, J.; Ruffieux, P.; Jaafar, R.; Passerone, D.; Feng, X.; Müllen, K.; Fasel, R.; Pignedoli, C. A. *ACS Nano* **2012**, *6*, 2020. (b) Huang, H.; Wei, D.; Sun, J.; Wong, S. L.; Feng, Y. P.; Neto, A. C.; Wee, A. T. S. *Sci. Rep.* **2012**, *2*, 983. (c) Dienel, T.; Kawai, S.; Söde, H.; Feng, X.; Müllen, K.; Ruffieux, P.; Fasel, R.; Gröning, O. *Nano Lett.* **2015**, *15*, 5185. (d) Chen, Y.-C.; Cao, T.; Chen, C.; Pedramrazi, Z.; Haberer, D.; de Oteyza, D. G.; Fischer, F. R.; Louie, S. G.; Crommie, M. F. *Nat. Nanotechnol.* **2015**, *10*, 156. (e) Liu, J.; Li, B.-W.; Tan, Y.; Giannakopoulos, A.; Sanchez-Sanchez, C.; Beljonne, D.; Ruffieux, P.; Fasel, R.; Feng, X.; Müllen, K. *J. Am. Chem. Soc.* **2015**, *137*, 6097.

(10) (a) Pinardi, A. L.; Otero-Irurueta, G.; Palacio, I.; Martinez, J. I.; Sanchez-Sanchez, C.; Tello, M.; Rogero, C.; Cossaro, A.; Preobrajenski, A.; Gómez-Lor, B. *ACS Nano* **2013**, *7*, 3676. (b) Pinardi, A. L.; Martínez, J. I.; Jančařík, A.; Stará, I. G.; Starý, I.; López, M. F.; Méndez, J.; Martín-Gago, J. Á. *Chem. Commun.* **2014**, *50*, 1555. (c) Liang, L.; Meunier, V. *J. Phys. Chem. C* **2015**, *119*, 775.

(11) Dienel, T.; Gómez-Díaz, J.; Seitsonen, A. P.; Widmer, R.; Iannuzzi, M.; Radican, K.; Sachdev, H.; Müllen, K.; Hutter, J.; Gröning, O. *ACS Nano* **2014**, *8*, 6571.

(12) (a) Usachov, D.; Vilkov, O.; Grüneis, A.; Haberer, D.; Fedorov, A.; Adamchuk, V. K.; Preobrajenski, A. B.; Dudin, P.; Barinov, A.; Oehzelt, M.; Laubschat, C.; Vyalikh, D. V. *Nano Lett.* **2011**, *11*, 5401. (b) Bronner, C.; Stremlau, S.; Gille, M.; Brauße, F.; Haase, A.; Hecht, S.; Tegeder, P. *Angew. Chem., Int. Ed.* **2013**, *52*, 4422.

(13) (a) Wiengarten, A.; Lloyd, J. A.; Seufert, K.; Reichert, J.; Auwärter, W.; Han, R.; Duncan, D. A.; Allegretti, F.; Fischer, S.; Oh, S. C.; Saglam, O.; Jiang, L.; Vijayaraghavan, S.; Écija, D.; Papageorgiou, A. C.; Barth, J. V. *Chem. - Eur. J.* **2015**, *21*, 12285. (b) Somorjai, G. A.; Park, J. Y. *Angew. Chem., Int. Ed.* **2008**, *47*, 9212. (c) Sun, Q.; Zhang, C.; Kong, H.; Tan, Q.; Xu, W. *Chem. Commun.* **2014**, *50*, 11825.

(14) Gottfried, J. M. *Surf. Sci. Rep.* **2015**, *70*, 259.

(15) Lafferentz, L.; Eberhardt, V.; Dri, C.; Africh, C.; Comelli, G.; Esch, F.; Hecht, S.; Grill, L. *Nat. Chem.* **2012**, *4*, 215.

(16) Björk, J.; Stafström, S.; Hanke, F. *J. Am. Chem. Soc.* **2011**, *133*, 14884.

(17) Gross, L.; Mohn, F.; Moll, N.; Liljeroth, P.; Meyer, G. *Science* **2009**, *325*, 1110.

(18) (a) Gross, L.; Mohn, F.; Moll, N.; Meyer, G.; Ebel, R.; Abdel-Mageed, W. M.; Jaspars, M. *Nat. Chem.* **2010**, *2*, 821. (b) Pavliček, N.; Fleury, B.; Neu, M.; Niedenführ, J.; Herranz-Lancho, C.; Ruben, M.; Repp, J. *Phys. Rev. Lett.* **2012**, *108*, 086101. (c) Hanssen, K. Ø.; Schuler, B.; Williams, A. J.; Demissie, T. B.; Hansen, E.; Andersen, J. H.; Svenson, J.; Blinov, K.; Repisky, M.; Mohn, F.; Meyer, G.; Svendsen, J.-S.; Ruud, K.; Elyashberg, M.; Gross, L.; Jaspars, M.; Isaksson, J. *Angew. Chem., Int. Ed.* **2012**, *124*, 12238. (d) Schuler, B.; Liu, S.-X.; Geng, Y.; Decurtins, S.; Meyer, G.; Gross, L. *Nano Lett.* **2014**, *14*, 3342.

(19) (a) Albrecht, F.; Neu, M.; Quest, C.; Swart, I.; Repp, J. *J. Am. Chem. Soc.* **2013**, *135*, 9200. (b) Albrecht, F.; Pavliček, N.; Herranz-Lancho, C.; Ruben, M.; Repp, J. *J. Am. Chem. Soc.* **2015**, *137*, 7424. (c) Mohn, F.; Repp, J.; Gross, L.; Meyer, G.; Dyer, M. S.; Persson, M. *Phys. Rev. Lett.* **2010**, *105*, 266102. (d) Riss, A.; Wickenburg, S.; Gorman, P.; Tan, L. Z.; Tsai, H.-Z.; de Oteyza, D. G.; Chen, Y.-C.; Bradley, A. J.; Ugeda, M. M.; Etkin, G.; Louie, S. G.; Fischer, F. R.; Crommie, M. F. *Nano Lett.* **2014**, *14*, 2251. (e) Hla, S.-W.; Bartels, L.; Meyer, G.; Rieder, K.-H. *Phys. Rev. Lett.* **2000**, *85*, 2777. (f) de Oteyza, D. G.; Gorman, P.; Chen, Y.-C.; Wickenburg, S.; Riss, A.; Mowbray, D.

J.; Etkin, G.; Pedramrazi, Z.; Tsai, H.-Z.; Rubio, A.; Crommie, M. F. *Science* **2013**, *340*, 1434.

(20) (a) Bergkamp, J.; Decurtins, S.; Liu, S.-X. *Chem. Soc. Rev.* **2015**, *44*, 863. (b) Liu, B.; Ran, Y.-F.; Li, Z.; Liu, S.-X.; Jia, C.; Decurtins, S.; Wandlowski, T. *Chem. - Eur. J.* **2010**, *16*, 5008. (c) Jia, C.; Liu, S.-X.; Tanner, C.; Leiggener, C.; Sanguinet, L.; Levillain, E.; Leutwyler, S.; Hauser, A.; Decurtins, S. *Chem. Commun.* **2006**, 1878. (d) Wu, J.; Dupont, N.; Liu, S.-X.; Neels, A.; Hauser, A.; Decurtins, S. *Chem. - Asian J.* **2009**, *4*, 392.

(21) Kocić, N.; Weiderer, P.; Keller, S.; Decurtins, S.; Liu, S.-X.; Repp, J. *Nano Lett.* **2015**, *15*, 4406.

(22) Abeywickrama, C.; Baker, A. D. *J. Org. Chem.* **2004**, *69*, 7741.

(23) (a) Fuchs, Y.; Lofters, S.; Dieter, T.; Shi, W.; Morgan, R.; Strekas, T. C.; Gafney, H. D.; Baker, A. D. *J. Am. Chem. Soc.* **1987**, *109*, 2691. (b) Grove, H.; Sletten, J.; Julve, M.; Lloret, F.; Cano, J. *J. Chem. Soc., Dalton Trans.* **2001**, 259. (c) Grove, H.; Sletten, J. *J. Chem. Crystallogr.* **2000**, *30*, 123. (d) González, I.; Dreyse, P.; Cortés-Arriagada, D.; Sundararajan, M.; Morgado, C.; Brito, I.; Roldán-Carmona, C.; Bolink, H. J.; Loeb, B. *Dalton Trans.* **2015**, *44*, 14771.

(24) Giessibl, F. J. *Appl. Phys. Lett.* **2000**, *76*, 1470.

(25) Soler, J. M.; Artacho, E.; Gale, J. D.; García, A.; Junquera, J.; Ordejón, P.; Sánchez-Portal, D. *J. Phys.: Condens. Matter* **2002**, *14*, 2745.

(26) Blum, V.; Gehrke, R.; Hanke, F.; Havu, P.; Havu, V.; Ren, X.; Reuter, K.; Scheffler, M. *Comput. Phys. Commun.* **2009**, *180*, 2175.

(27) Tkatchenko, A.; Scheffler, M. *Phys. Rev. Lett.* **2009**, *102*, 073005.

(28) Hapala, P.; Kichin, G.; Wagner, C.; Tautz, F. S.; Temirov, R.; Jelínek, P. *Phys. Rev. B: Condens. Matter Mater. Phys.* **2014**, *90*, 085421.

(29) Hapala, P.; Temirov, R.; Tautz, F. S.; Jelínek, P. *Phys. Rev. Lett.* **2014**, *113*, 226101.

(30) Giessibl, F. J. *Appl. Phys. Lett.* **2001**, *78*, 123.

(31) Kawai, S.; Saito, S.; Osumi, S.; Yamaguchi, S.; Foster, A. S.; Spijker, P.; Meyer, E. *Nat. Commun.* **2015**, *6*, 8098.

(32) (a) Neu, M.; Moll, N.; Gross, L.; Meyer, G.; Giessibl, F. J.; Repp, J. *Phys. Rev. B: Condens. Matter Mater. Phys.* **2014**, *89*, 205407. (b) Moll, N.; Schuler, B.; Kawai, S.; Xu, F.; Peng, L.; Orita, A.; Otera, J.; Curioni, A.; Neu, M.; Repp, J. *Nano Lett.* **2014**, *14*, 6127.

(33) (a) Shi, Z.; Lin, N. *J. Am. Chem. Soc.* **2009**, *131*, 5376. (b) Maksymovych, P.; Sorescu, D. C.; Yates, J. T., Jr *Phys. Rev. Lett.* **2006**, *97*, 146103. (c) Stepanow, S.; Lin, N.; Payer, D.; Schlickum, U.; Klappenberger, F.; Zoppellaro, G.; Ruben, M.; Brune, H.; Barth, J. V.; Kern, K. *Angew. Chem.* **2007**, *119*, 724. (d) Pawin, G.; Wong, K. L.; Kim, D.; Sun, D.; Bartels, L.; Hong, S.; Rahman, T. S.; Carp, R.; Marsella, M. *Angew. Chem., Int. Ed.* **2008**, *47*, 8442. (e) Mielke, J.; Hanke, F.; Peters, M. V.; Hecht, S.; Persson, M.; Grill, L. *J. Am. Chem. Soc.* **2015**, *137*, 1844. (f) Yang, Z.; Corso, M.; Robles, R.; Lotze, C.; Fitzner, R.; Mena-Osteritz, E.; Bäuerle, P.; Franke, K. J.; Pascual, J. I. *ACS Nano* **2014**, *8*, 10715.

(34) Hämäläinen, S. K.; van der Heijden, N.; van der Lit, J.; den Hartog, S.; Liljeroth, P.; Swart, I. *Phys. Rev. Lett.* **2014**, *113*, 186102.

(35) van der Lit, J.; Di Cicco, F.; Prokop, H.; Jelínek, P.; Swart, I. *Phys. Rev. Lett.* **2016**, *116*, 0961012.

(36) Ran, Y.-F.; Liu, S.-X.; Sereda, O.; Neels, A.; Decurtins, S. *Dalton Trans.* **2011**, *40*, 8193.

(37) There are a few observations of bonds that could not be unambiguously identified. We therefore provide an upper limit of at most 2% of pyridine−pyridine bonded structures.

(38) (a) Sweetman, A.; Jarvis, S.; Sang, H.; Lekkas, I.; Rahe, P.; Wang, Y.; Wang, J.; Champness, N.; Kantorovich, L.; Moriarty, P. *Nat. Commun.* **2014**, *5*, 3931. (b) Pavliček, N.; Herranz-Lancho, C.; Fleury, B.; Neu, M.; Niedenführ, J.; Ruben, M.; Repp, J. *Phys. Status Solidi B* **2013**, *250*, 2424.